Effect of antimony concentration on optical, electrical and structural properties of copper antimony sulphide thin films deposited by spray pyrolysis technique

N Obare[1], M Mageto [1, 2], and V Odari1 [2]

1. Department of Physics, Masinde Muliro University of Science and Technology, P.O Box 190-50100, Kakamega, Kenya.
2. Materials Research Society of Kenya, P.O. Box 15653-00503 Nairobi, Kenya.

E-mail: nancymoraamonantia@gmail.com

Abstract

Copper antimony sulphide ($CuSbS_2$) is a semiconductor with narrow band gap and a potential absorber material for applications in various optoelectronic devices like infrared detectors and solar cells. In this paper, $CuSbS_2$ thin films were deposited by spray pyrolysis technique on glass substrates at a temperature of $3000\,°C$, using cupric chloride, antimony chloride, and thiourea as precursors. The samples were prepared by varying the antimony concentration (0.1M, 0.15M, and 0.2M) at a pressure of 3.5 bar and a solution flow rate of 2 ml/min for 5 minutes, while the precursor solutions of Cu:S molar ratio (0.1:0.2) was maintained. Elemental, morphological, optical, and structural characterization of these films was done from data obtained from energy dispersive X-ray fluorescence (EDXRF), UV-VIS spectrophotometer, scanning electron microscope (SEM) and X-Ray diffraction (XRD) respectively. The prepared thin films were polycrystalline with a preferential peak at (111). Electrical properties of the thin films were obtained by simulating the UV-VIS spectra in SCOUT software using the Drude and Kim oscillator model. Deposited films have a band gap range of 1.84 – 1.98 eV, conductivity range of 199.59 – 204.67 $\Omega^{-1}cm^{-1}$, and carrier concentration range of $1.12×10^{19}$ - $1.27×10^{19}$ cm^{-3}.

Keywords: spray pyrolysis, thin films, $CuSbS_2$, antimony cocemtration, SCOUT

1. Introduction

Solar energy is an important and sustainable renewable energy source to meet the rapidly growing energy need [1]. This energy is converted into electrical energy by the use of photovoltaic cells. Among the various types of solar cells developed so far, thin film photovoltaic is the most promising technology to bring change to the photovoltaic industry which is currently relying on Si-based solar cells [2]. Solar energy technologies and applications are growing rapidly owing to the fact that the sun is a clean, free and sustainable source [3]. The rising energy need and the short coming of existing technologies because of the scarcity, cost, and toxicity of the materials have led researchers to look for alternative materials for thin film solar cells based on earth-abundant, inexpensive and less toxic materials [4,5].

The investigation of an upcoming diverse ternary thin film of copper-based chalcogenide semiconductors and p-type photo-absorber layer are done for thin film solar cells which are based on non-toxic, earth abundant and relatively cheap materials, [6]. Copper antimony sulphide ($CuSbS_2$) is a semiconductor with narrow band gap ability in applications in various optoelectronic devices such as infrared detectors and solar cells as reported by [6], [7] and [8]. It possesses an optical band gap of 1.5 eV, the optimum value for an absorber material in solar cells [9], a high absorption coefficient of 10^5 cm^{-1} [10], tenable hole concentration in a range of $10^{16} – 10^{18}$ cm^{-1} [8], and hole mobility of 49 cm^2/Vs [11]. This semiconductor has a potential to substitute rare and expensive indium and gallium semiconductors in thin film solar cells. Important to note, the ionic radius of indium and antimony are almost equal, 80 and 76 pm, respectively [2].

$CuSbS_2$ exhibits p-type semiconducting nature [12], in comparison with the existing absorber materials like Cadmium telluride, Copper Indium Selenide, Copper Indium Gallium Selenide having advantages of low

toxicity [13]. $CuSbS_2$ are of earth abundant and economically adoptable for low-cost device fabrication and eco-friendly manner [14]. $CuSbS_2$ thin films have been deposited by various methods such as Spray Pyrolysis [15] Thermal Evaporation [5], [12], chemical bath deposition, [16], [17] Electro Chemical Deposition [18], [19] solvothermal method [20] spin coating technique and self-regulated growth as reported by [21].

In this work, efforts were made to deposit thin films of $CuSbS_2$ on a glass substrates using the spray pyrolysis method by varying the antimony concentration with the aim of exploring its properties as an absorber layer. They were characterized using X-ray diffraction (XRD), scanning electron microscopy (SEM), UV spectrophotometry, energy dispersive X-ray fluorescence, and SCOUT 2 software.

2. Experiment
2. 1. Sample preparation
Glass substrates were cleaned in a sonicator containing isopropanol for 15 minutes and the procedure was repeated using distilled water and acetone, then dried on a hot plate at a temperature of 30-35°C. Precursor preparation procedure was adopted from [9] by separately dissolving 1.366g of $SbCl_3$, 0.511g of $CuCl_2$, and 0.9134g of $SC(NH_2)_2$, all analytical grade, in 60 ml isopropanol each. Samples were prepared at precursor molar ratios of Cu:Sb:S [0.1:0.1:0.2], while maintaining cupric chloride and antimony chloride precursor ratio equal. Trials were done with the variation of thiourea molar ratio. Relatively good quality thin films were formed when thiourea was twice as cupric chloride, this variation of thiourea was to maintain the stoichiometry. It was noted that, at lower concentrations of thiourea, the films were not formed and at higher concentrations, the solution was precipitated. Due to the partial solubility of $CuCl_2$ in isopropanol, the cupric chloride concentration variation in the solution was very limited. We realized that as cupric chloride was increased, the thiourea concentration was also to be increased slightly to avoid the precipitation in the solution. The concentration ratio of both $CuCl_2$ and thiourea in isopropanol was therefore fixed at 1:2. The precursor solutions were sprayed at a flow rate of 2 ml/min for 5 minutes, deposition pressure of 3.5 bar, nozzle to glass substrate, vertical distance of 15 cm, and 60 cm horizontally. The temperature was kept at 300°C and antimony concentration was varied (0.1M, 0.15M, 0.2M) while copper and sulphur was maintained at 0.1M and 0.2M, respectively. The schematic diagram of the spray chamber is as shown in figure. 1

2. 2. Sample characterization
X-ray diffraction (XRD) patterns were recorded by Bruker D2-phaser diffractometer using Cu Kα_1 radiation (λ=1.54059 Å), the glazing incident angle was in parallel beam geometry with the diffraction angle 1° while scan range (2θ) was 20 to 80°.

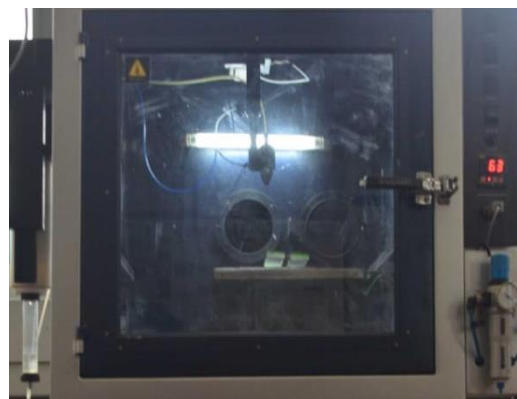The Rigaku NEX CG Energy Dispersive X-Ray fluorescence was used for elemental analysis, Zeiss

Figure 1. Schematic diagram of a spray chamber.

Crossbeam 540 FEG SEM was used to give clear images of the deposited copper antimony sulphide thin films. The images enabled us to check the morphology at different antimony concentrations. SCOUT 2 software was used to determine the electrical properties and the optical measurement was performed with a 100 BIO UV-Vis spectrometer.

2. 3 Determination of electrical properties and optical constants
The dispersion analysis involving Drude and Kim terms in SCOUT 2 software was used to determine the film thickness in a wavelength range 200-800 nm by fitting the experimental spectral data to the theoretical spectral data. From the fitted spectrum, the thickness of the three samples were approximated to be 150 nm.

Drude model, which has the plasma frequency (Ω_p) and damping constant (γ) parameters and Kim oscillator model is used to simulate the measured absorbance and transmittance [22], the models are expressed as a function of frequency ω, as follows:

$$\chi_{Drude}(\omega) = \frac{\Omega_p^2}{\omega^2 + i\omega\gamma} . \tag{1}$$

Resonance frequency ω, oscillator strength Ω_p damping constant γ, and the Gauss–Lorentz-switch constant σ are four adjustable parameters developed by Kim and the interband dielectric susceptibility is described by:

$$\chi_{kim} = \frac{\Omega_p^2}{\Omega_0^2 - \omega^2 - i\omega\gamma} . \tag{2}$$

The thin film optical constants and thickness of the prepared samples were determined from the best fits between computed and experimental data using Scout 2 software.

3. Results and discussion
3. 1. X-Ray diffraction analysis
The XRD patterns of the deposited $CuSbS_2$ thin films at varied antimony concentration are shown in figure. 2 (a), (b), and (c). The XRD patterns were recorded for all films in the range of diffraction angle 2θ between 20^0 and 80^0. The analysis and identification of phase of the thin films were indexed with standard data ICDD Card
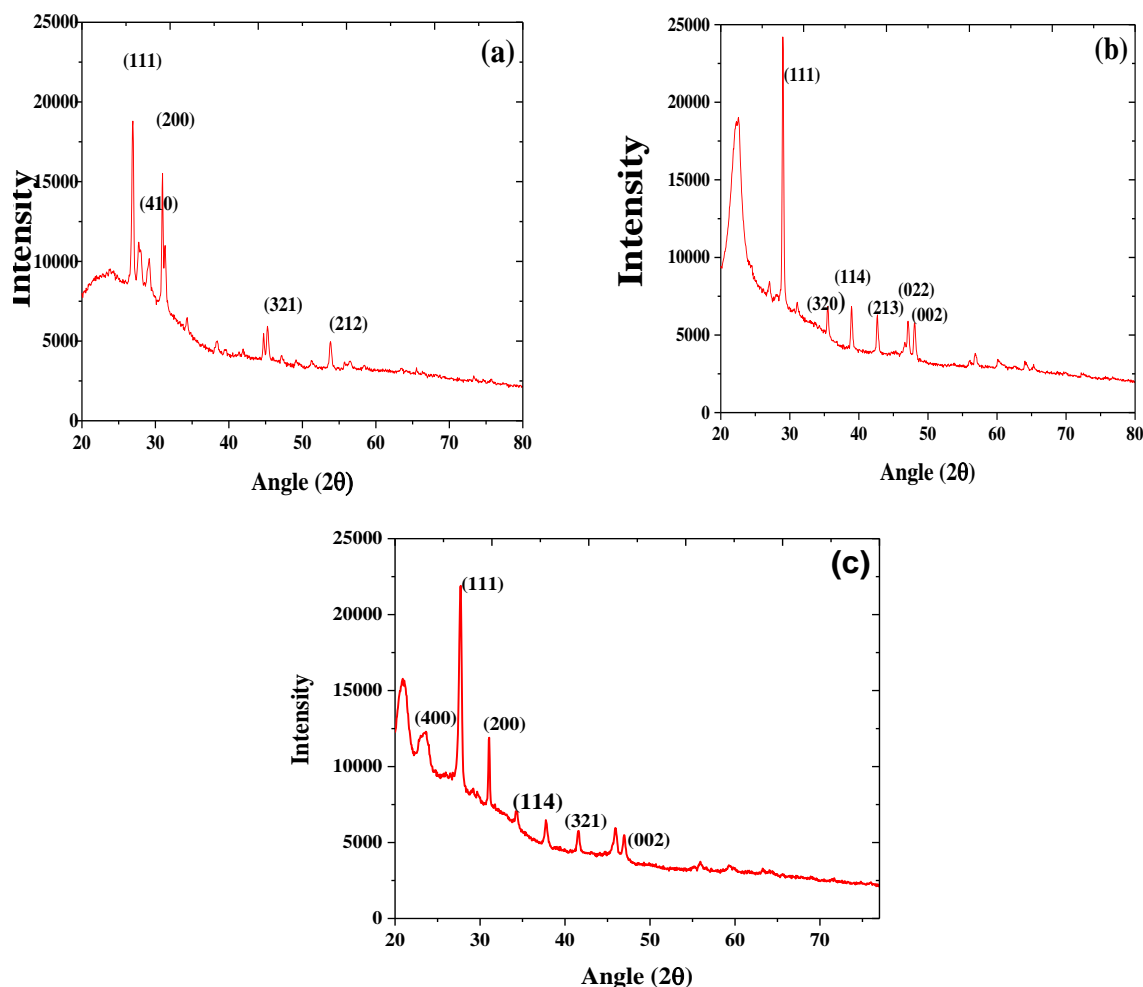
Figure 2. XRD pattern for samples deposited at varied antimony concentration.
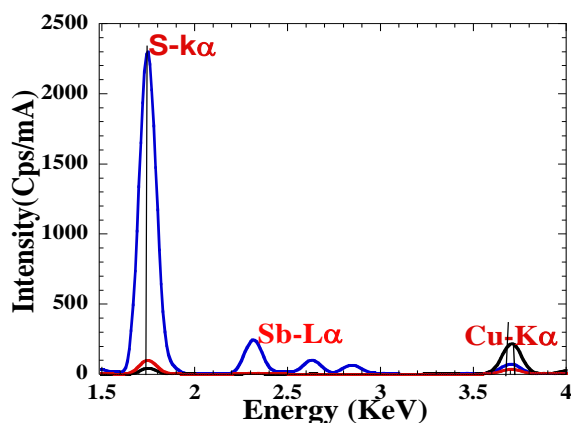

Figure 3. Spectra of elemental composition of CuSbS₂ using RX9, Cu, and Mo targets.

No: 44-1417. The X-ray diffraction pattern of these films revealed that CuSbS₂ films have polycrystalline phases.

From the XRD pattern, the major diffraction peaks at 2θ were 28.44, 35.09, 39.63, 42.61, 47.21, and 54.51, identified as reflection planes from (111), (220), (320), (221), (321) (002) and (402) of orthorhombic crystal structure of chalcostibite phase. As the antimony concentration were increased, the peak intensity also increased, implying that there is high degree of crystallization as the concentration of antimony

increased. The crystalline size was calculated using the Scherrer's formula [23] on the preferential (111) peak:

$$D = \frac{0.9\lambda}{\beta\cos\theta}, \tag{3}$$

At the concentration of antimony of 0.1M, 0.15M, and 0.2M, the crystallite size was found to be increasing from 25.00 nm, 35.86 nm, and 38.85 nm, respectively. The increase in grain size implies that the thin film became more stable and there is a reduction of strain with increasing antimony concentration.

3. 2 Energy Dispersive X-Ray Florescent

The elemental composition of the fabricated thin films prepared was done by energy dispersive x-ray fluorescence. EDXRF uses high energy x-rays to excite fluorescent radiation from a sample for elemental or chemical analysis [24]. The fitted spectrum consists of the sum of individually generated profiles using the response function for each element obtained by the full profile (FP) method. Quantification results were obtained by iteratively adjusting the fitted spectrum until it matched the measured spectrum. The result showing the elemental composition of CuSbS₂ is shown in figure 3. To obtain the optimal excitation conditions, RX9, Cu, and Mo secondary targets were used.
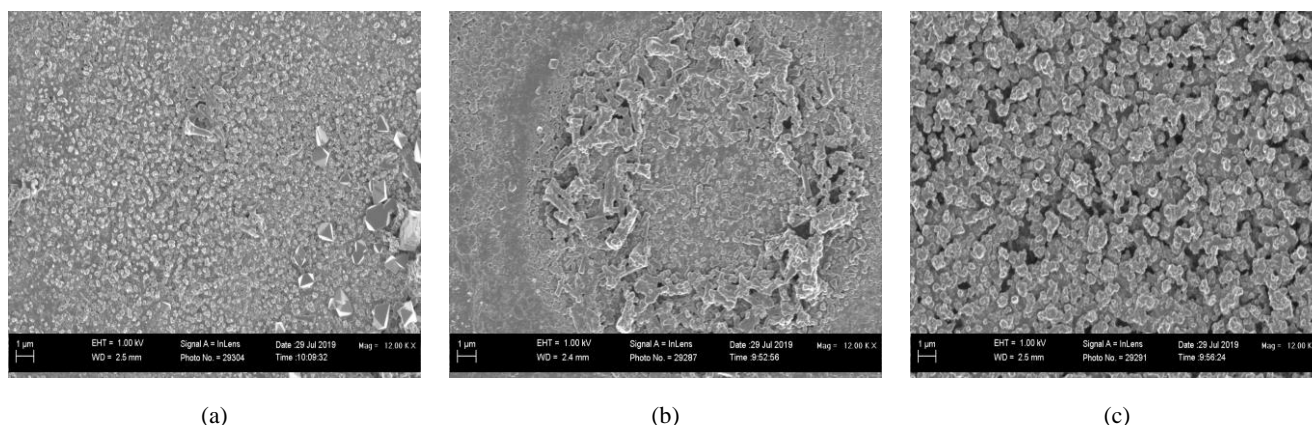
(a) (b) (c)

Figure 4. SEM images for variation of antimony concentration a) 0.1M b) 0.15M c) 0.2M.

From figure 3, the spectra of $CuSbS_2$ measured by Mo, Cu, and RX9 secondary targets showed that the sample contained 23000ppm of copper, 69400ppm of antimony and 282000ppm of Sulphur. The spectrum measured with RX9 secondary target shows the escape peak of $SK\alpha$ appears at 1.75Kev, Cu secondary target escape of $Sb-L\alpha$ at 2.20keV and Mo secondary shows escape peak of $Cu-K\alpha$ at 11.3keV. Therefore, the sample prepared contained Copper, Antimony, and Sulphur. The EDXRF results indicate the molarity ratio of Cu:Sb:S present in the samples to be 1:1:2. Implying that the thin film prepared is copper antimony sulphide.

3. 3 Morphology
Scanning Electron Microscopy (SEM) was used to study the microstructure of the prepared samples because it is a suitable and adaptable method to produce magnified images which enabled us to examine the growth pattern [12]. The SEM images of $CuSbS_2$ thin films prepared at different antimony concentration are shown in figure 4. It is seen that copper antimony sulphide deposited at molar concentration of 0.1M shows interconnected irregular shaped particles. At the molar concentration of 0.15M, a more compact morphology with better grains is seen. Films with bigger grains and definite boundaries are formed when the antimony concentration was increased to 0.2M.

3. 4 Optical properties
The optical measurements of the prepared samples were done by UV-VIS spectrophotometer in the wavelength range of $200 \leq \lambda \leq 800$ nm. The absorbance, transmittance, and optical band gap of the films were calculated using the Tauc plots based on the standard formula:

$$(\alpha h\nu)^n = A(h\nu - E_g), \tag{4}$$

where α is the absorption coefficient corresponding to the energy $h\nu$, h is the Plank's constant, ν is the frequency, and A is a constant. The value of n equals to 2 for an allowed direct, 1/2 for an allowed indirect, and 2/3 for forbidden transition [9]. Absorption coefficient (α) in the absorbance region was calculated using equation 5

similar to the work done by [25].

$$\alpha = \frac{1}{d}\ln\left(\frac{1-R}{T}\right), \tag{5}$$

where, d is the thin film thickness, R is the reflectance, and T is the transmittance. A good linear fit of $(\alpha h\nu)^2$ verses $h\nu$ was obtained for $n=2$ (direct allowed transition) for all $CuSbS_2$ thin films, which implies that the fundamental optical absorption is dominated by the direct allowed transitions [26].

The absorption coefficients of copper antimony sulphide samples are 10^6 cm^{-1} on the films deposited at 0.15M and 0.2M antimony concentration, these high absorption coefficients together with well-suited band gaps make the copper antimony sulphide thin film good for photovoltaic applications, because the high absorption implies that the film are ready to absorb photons that excites electrons into the conduction band thus enabling it to be a good absorbing material. The films show a broad absorption over a wide wavelength range. The band gap was obtained for $CuSbS_2$ films by extrapolation of a straight line to the energy axis. The intercept of the straight line to the energy axis $(X - axis)$ directly gave the optical band gap values of antimony concentration of 0.1M, 0.15M, and 0.2M as 1.84 eV, 1.92 eV, and 1.96 eV respectively [4] as shown in figure 5(a-c). Due to modification of the conduction band and valence band to various extents with increasing antimony concentration, it caused the absorption edge to be pushed to higher energies because of some states being closer to the conduction band therefore resulting in the increase of band gap with the increase of antimony concentration. These high absorption coefficients together with well-suited band gaps make both phases good for PV applications.

3. 5 Electrical properties
The electrical properties of the thin films were simulated using SCOUT 2 software. The simulated spectra of the model were fit to the measured data. The carrier concentration, mobility, and resistivity were then computed similar to [22]. The Drude model relates the macroscopic susceptibility to the microscopic quantities
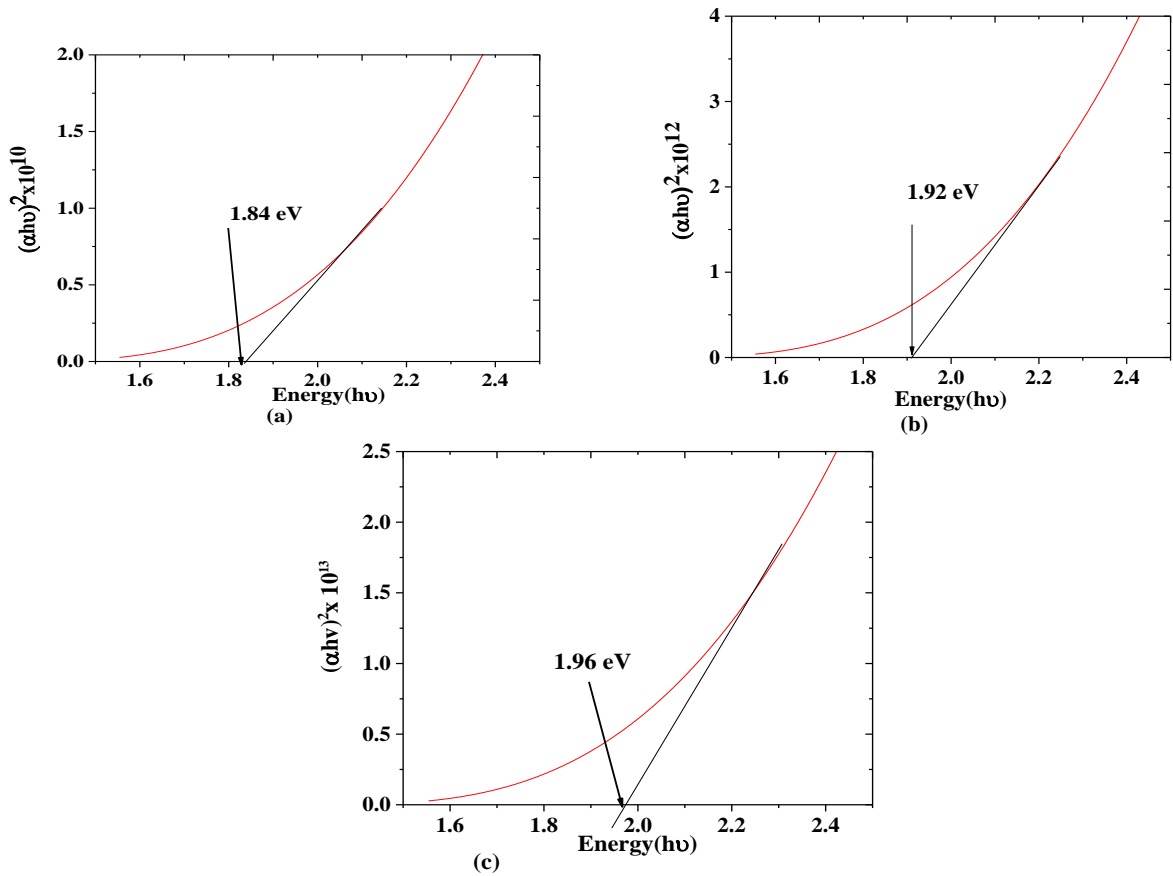
Figure 5. Band gap of CuSbS₂ at varied molar concentration antimony (a) 0.1M, (b) 0.15M, (c) 0.2M while maintaining copper: sulphur at 0.1M: 0.2M, (d) absorption coefficient and (e) Refractive index with wavelength.

Table 1. Calculated values of Drude and Kim model parameters, carrier concentration (n), mobility (μ), and resistivity at varied antimony concentration.

Films	Plasma frequency(Ω_p)cm⁻¹	Damping constant(Ω_τ)cm⁻¹	Carrier concentration (n)cm⁻³	Mobility (μ) cm²/Vs	Resistivity(ρ) Ωcm	Conductivity (σ) Ω⁻¹cm⁻¹
0.1M Sb	1462.2871	178.8463	1.12×10^{19}	1.768×10^{19}	0.00501	199.59
0.15M Sb	1546.6653	196.6928	1.25×10^{19}	1.6×10^{19}	0.00493	203.038
0.2M Sb	1559.0544	198.2625	1.27×10^{19}	1.59×10^{19}	0.00488	204.67

carrier concentration n and mobility μ as given by Equation 6 and 7, respectively.

$$n = \frac{4\pi^2 c_0{}^2 \varepsilon_0 m}{e^2}\Omega_p^2, \tag{6}$$

$$\mu = \frac{e}{2\pi m c \Omega_\tau^2}, \tag{7}$$

Resistivity was calculated by using:

$$\rho = \frac{\Omega_\tau}{2\pi c \varepsilon_0 \Omega_p^2}, \tag{8}$$

where Ω_τ is the damping constant, Ω_p is the plasma frequency, e is the elementary charge, ε_0 is the permittivity of the free space, and $m=0.47m_e$ the effective mass of the charge carrier and m_e is the mass of an electron [27].

The conductivity of the investigated thin films increases with antimony concentration similar with the work reported by [28]. From the results, it implies that the carrier concentration increases with increasing concentration of antimony. Because of the increase in carrier concentration, it leads to filling of the conduction band, blocking the lowest energy states, thus enabling the transition to occur at higher levels leading to the increase in the band gap with an increase of antimony concentration. The higher mobility of 10^{19} m²/vs of the thin films (table 1) suggests that copper antimony sulphide is a good absorber material for solar cell applications.

4. Conclusions

The CuSbS₂ thin films were deposited on glass substrates with varied antimony concentration (0.1M, 0.15M, 0.2M), at temperature of 300 ℃, pressure of 3.5 bar, and flowrate of 2 ml/min for 5 minutes, by using spray pyrolysis. SEM results revealed that the interconnected irregular shaped particles were observed at 0.1M, but with increasing antimony concentration films with bigger grains and definite boundaries were formed. XRD analysis confirms the thin films crystallized in an orthorhombic system. The presence of

each constituent element in the deposited thin films were detected by EDXRF studies. Optical absorption spectral analysis described the absorption nature of the films, further, the band gap broadening was achieved by increasing the antimony concentration, and also the band gap of $CuSbS_2$ film were found to be 1.84 eV and it increased to 1.98 eV for the film prepared at 0.2M of antimony concentration.

References

1. S Suehiro, *et al*., *Inorganic Chemistry* **54**, 16 (2015) 7840.
2. S Thiruvenkadam and A L Rajesh, *International Journal of Scientific and Engineering Research* **3** (2014) 38.
3. T Rath, *et al*., *Journal of* Materials *Chemistry* A **3**, 47 (2015) 24155.
4. S A Manolache and A Duta, *Journal of Optoelectronics and Advanced Materials* **9**, 10 (2007) 3219.
5. F W de Souza Lucas, *et al*., *The Journal of Physical Chemistry* C **120**, 33 (2016) 18377.
6. Y Rodrıguez Lazcano, M T S Nair, and P K Nair, *Journal of Crystal Growth* **223**, 3 (2001) 399.
7. A Rabhi, M Kanzari, and B Rezig, *Materials Letters* **62**, 20 (2008) 3576.
8. A Rabhi, M Kanzari, and B Rezig, *Thin Solid Films* **517**, 7 (2009) 2477.
9. J A Ramos Aquino, *et al*., *Physica Status Solidi* (c) **13**, 1 (2016) 24.
10. Sh Banu, *et al*., *Solar Energy Materials and Solar Cells* **151** (2016) 14.
11. W Septina, *et al*., *Thin Solid Films* **550** (2014) 700.
12. R Suriakarthick, *et al*., *Journal of Alloys and Compounds* **651** (2015) 423.
13. L Wan, *et al*., *Journal of Alloys and Compounds* **680** (2016) 182.
14. B Krishnan, S Shaji, and R Ernesto Ornelas, *Journal of Materials Science: Materials in Electronics* **26**, 7 (2015) 4770.
15. S Manolache, *et al*., *Thin Solid Films* **515**, 15 (2007) 5957.
16. A I Onyia, *Journal of Non-Oxide Glasses* **8**, 4 (2017) 99.
17. V Vinayakumar, *et al*., *RSC Advances* **8**, 54 (2018) 31055.
18. A C Rastogi and N. R. Janardhana, *Thin Solid Films* **565** (2014) 285.
19. D Colombara, *et al*., *Thin Solid Films* **519**, 21 (2011) 7438.
20. T Manimozhi, *et al*., *Materials Science in Semiconductor Processing* **103** (2019) 104606.
21. A W Welch, *et al*., *Solar Energy Materials and Solar Cells* **132** (2015) 499.
22. W Thesis, *"Scout Thin Film Analysis Software Handbook, Hard- and Software",* Aachen Germany (2001)
23. B Ingham and M F Toney, "*Metallic Films for Electronic, Optical and Magnetic Applications*" Woodhead Publishing (2014).
24. T Moriyama, *et al*., *Rigaku Journal* **29**, 2 (2013) 27.
25. C G Granqvist, "*Handbook of inorganic electrochromic materials*" Elsevier (1995).
26. C Garza, *et al*., *Solar Energy Materials and Solar Cells* **95**, 8 (2010) 2001.
27. M Birkett, *et al*., *APL Materials* **6**, 8 (2018) 084904.
28. M E Edley, *et al*., *Thin Solid Films* **646** (2017) 180.